

# Finite-temperature effects in magnetic dipole transitions

---

Kaur, Amandeep; Yüksel, Esra; Paar, Nils

Source / Izvornik: **Physical Review C, 2024, 109**

Journal article, Published version

Rad u časopisu, Objavljena verzija rada (izdavačev PDF)

<https://doi.org/10.1103/PhysRevC.109.024305>

Permanent link / Trajna poveznica: <https://urn.nsk.hr/urn:nbn:hr:217:241410>

Rights / Prava: [In copyright](#) / [Zaštićeno autorskim pravom.](#)

Download date / Datum preuzimanja: **2025-02-01**






Repository / Repozitorij:

[Repository of the Faculty of Science - University of Zagreb](#)



## Finite-temperature effects in magnetic dipole transitions

Amandeep Kaur <sup>1,\*</sup>, Esra Yüksel <sup>2,†</sup> and Nils Paar <sup>1,‡</sup>

<sup>1</sup>*Department of Physics, Faculty of Science, University of Zagreb, Bijenička Cesta 32, 10000 Zagreb, Croatia*

<sup>2</sup>*Department of Physics, University of Surrey, Guildford, Surrey GU2 7XH, United Kingdom*



(Received 13 October 2023; accepted 22 January 2024; published 6 February 2024)

Finite-temperature effects in electromagnetic transitions in nuclei contribute to many aspects of nuclear structure and astrophysically relevant nuclear reactions. While electric dipole transitions have already been extensively studied, the temperature sensitivity of magnetic transitions remains largely unknown. This work comprises the study of isovector magnetic dipole excitations ( $M1$ ) occurring between spin-orbit (SO) partner states using the recently developed self-consistent finite-temperature relativistic quasiparticle random-phase approximation (FT-RQRPA) in the temperature range from  $T = 0$  to 2 MeV. The  $M1$  strength distributions of  $^{40-60}\text{Ca}$  and  $^{100-140}\text{Sn}$  isotopic chains exhibit a considerable temperature dependence. The  $M1$  strength peaks shift significantly towards the lower energies due to the decrease in SO splitting energies and weakening of the residual interaction, especially above the critical temperatures where the pairing correlations vanish. By exploring the relevant two-quasiparticle configurations contributing to the  $M1$  strength of closed- and open-shell nuclei, new proton and neutron excitation channels between SO partners are observed in low- and high-energy regions due to the thermal unblocking effects around the Fermi level. At higher temperatures, we have noticed an interesting result in  $^{40,60}\text{Ca}$  nuclei, the appearance of  $M1$  excitations, which are forbidden at zero temperature due to fully occupied (or fully vacant) spin-orbit partner states.

DOI: [10.1103/PhysRevC.109.024305](https://doi.org/10.1103/PhysRevC.109.024305)

### I. INTRODUCTION

A comprehensive understanding of the magnetic dipole ( $M1$ ) nuclear response is essential to various aspects of nuclear structure phenomena, such as isospin-mixing, isospin-splitting, and ground-state correlations [1–3]. It also aids in the study of radiative neutron capture, which has a key role in the production of neutron-rich elements in hot stellar environments [4–7]. Several experimental and theoretical studies have revealed intriguing behavior in  $\gamma$ -ray strength functions ( $\gamma$ SFs), and a notable enhancement is observed in the strength function toward lower transition energies [8–15]. The fine structure of strength functions in the  $E_\gamma = 5$ –8 MeV region is generally determined using the low-energy part of the electric dipole ( $E1$ ) response; however, some studies also suggest an anomalous increase below 4 MeV in the  $\gamma$ SF, which is attributed to the  $M1$  strength [16–19]. Thus, more research is required to explore the role of  $M1$  excitations in the  $\gamma$ SF. The  $M1$  spin-flip excitations are obtained at higher excitation energies around 8 MeV, which has so far been difficult to measure experimentally [1]. Furthermore, the so-called scissors mode of  $M1$  excitations in deformed nuclei was initially proposed in Ref. [20] and later observed at energies around 3 MeV. This observation is attributed to the scissorlike motion of neutrons and protons relative to each other [21–23].

$M1$  excitations exhibit a wide range of characteristics related to their energies, transition strengths, and decay properties, which are expected to be sensitive to the extreme conditions of temperature ( $T$ ), isospin ( $N/Z$ ), and deformation ( $\beta$ ) of nuclei. Recently, the relativistic quasiparticle random-phase approximation (RQRPA) has been utilized to investigate the role of residual interaction, spin-orbit (SO) splitting, pairing correlations, and neutron excess in the  $M1$  response [24–28]. Temperature can also significantly impact the electromagnetic nuclear response, which in turn modifies astrophysically relevant quantities such as neutron capture cross section, nuclear reaction rates, and element abundances. However, the measurement of  $M1$  transitions in highly excited nuclei poses a substantial challenge from an experimental standpoint. Previous studies of excitations in hot nuclei have considered mainly electric giant dipole resonance [29,30], primarily based on measurements of  $\gamma$  decay following fusion reactions induced by heavy-ion collisions [31], or alternatively by inelastic scattering of  $\alpha$  particles [32,33] or  $\alpha$ -induced fusion reactions [34]. From the decay of the compound nucleus, one could, at least in principle, also investigate  $M1$  emissions at finite temperature. However, to detect typically low-yield and complex  $M1$  emissions, highly efficient  $\gamma$  detector arrays with high-energy resolution would be required. The Oslo method could also be useful to extract  $\gamma$  rays associated with  $M1$  emissions from nuclei at high-excitation energies produced in transfer and inelastic scattering reactions with light ions, up to the neutron (proton) threshold [35,36]. Given the challenges associated with experimental studies, theoretical calculations become a more

\*akaur.phy@pmf.hr

†e.yuksel@surrey.ac.uk

‡npar@phy.hr

feasible and practical approach to study these excitations in hot nuclei.

In previous studies, temperature effects in electric multipole excitations have been investigated using several extensions of the random-phase approximation (RPA) [37–42]. The finite-temperature quasiparticle RPA based on the Skyrme functional has been used in studies of the electric multipole responses of hot nuclei in Refs. [38–40]. A self-consistent finite-temperature relativistic RPA (FT-RRPA), based on meson-exchange interaction, has been successfully employed to study the evolution of isoscalar and isovector electric multipole modes with temperature; however, the pairing correlations were not implemented in this approach [41]. Furthermore, finite-temperature relativistic time-blocking approximation (FT-RTBA) approach, based on Matsubara Green's function formalism, has been developed to investigate the electric nuclear response in excited nuclei [43,44]. Lately, electromagnetic strength distributions in both closed-shell and open-shell nuclei have been obtained from first principles at zero and finite temperatures, taking into account pairing and deformation effects [15]. Additionally, a self-consistent finite-temperature relativistic quasiparticle RPA (FT-RQRPA) has been introduced for non-charge-exchange excitations at finite temperatures, which also includes pairing correlations to address open-shell nuclei [45]. It has been employed to study the thermal effects on isovector  $E1$  excitations, demonstrating how the isovector giant dipole resonance and low-energy dipole excitations evolve with increasing temperature. It has been shown that new low-energy states appear due to the thermal unblocking effects. Consequently, the FT-RQRPA provides new perspectives for the microscopic calculation of  $\gamma$ SFs at finite temperatures associated with nuclear phenomena in stellar environments. Therefore, it is of particular interest to analyze the thermal effects on  $M1$  excitations as well as their contributions to  $\gamma$ SFs relevant for nucleosynthesis. In this work, we focus on  $M1$  excitations, characterized by unnatural parity transitions, for which additional modifications of the residual FT-RQRPA interaction are required. More details about the RQRPA formalism for magnetic transitions and their properties in the zero-temperature limit can be found in Refs. [24–28,46].

The novelty of the present study lies in its exploration of the temperature dependence of isovector (IV)  $M1$  ( $J^\pi = 1^+$ ) excitations using the newly developed FT-RQRPA framework for nuclei in the  $^{40-60}\text{Ca}$  and  $^{100-140}\text{Sn}$  isotopic chains. To study the unnatural parity excitations of  $M1$  type, the FT-RQRPA residual interaction is further extended by introducing the relativistic isovector-pseudovector (IV-PV) contact interaction [26]. The primary goals of this work are (i) to investigate the evolution of  $M1$  strength distributions with increasing temperature and isospin of nuclei, (ii) to study the impact of temperature on the SO splitting energies and their relation with the  $M1$  nuclear response, (iii) to examine the isovector  $M1$  non-energy-weighted and energy-weighted summations as a function of temperature and mass number, and (iv) to identify the new  $M1$  proton and neutron excitations in the low-energy as well as the high-energy region.

The paper is organized as follows: a brief description of the FT-RQRPA framework used in this study is given in

Sec. II. The extension of the residual interaction for unnatural parity  $M1$  excitations is explained. Section III presents the FT-RQRPA results and discussions of  $M1$  excitations in Ca and Sn isotopic chains in the temperature range  $T = 0-2$  MeV. Finally, a summary of the results and conclusions are outlined in Sec. IV.

## II. METHODOLOGY

In this work, we extend the FT-RQRPA from Ref. [45] for the study of unnatural parity excitation of  $M1$  type. The nuclear properties are described within the finite-temperature Hartree-Bardeen-Cooper-Schrieffer (FT-HBCS) framework [47,48]. In both the FT-HBCS and FT-RQRPA frameworks, the relativistic energy density functional (REDF) with point coupling DD-PCX interaction is implemented [49]. The point-coupling REDF is determined from the Lagrangian density,

$$\mathcal{L} = \mathcal{L}_{\text{PC}} + \mathcal{L}_{\text{IV-PV}}, \quad (1)$$

where  $\mathcal{L}_{\text{PC}}$  includes fermion contact interaction terms as isoscalar-scalar, isoscalar-vector, and isovector-vector channels (for detailed information, see Refs. [49,50]). The Lagrangian density (1) also includes the relativistic isovector-pseudovector (IV-PV) contact interaction, which is necessary for the FT-RQRPA residual interaction for the unnatural parity excitations of the  $M1$  type [26],

$$\mathcal{L}_{\text{IV-PV}} = -\frac{1}{2}\alpha_{\text{IV-PV}}[\bar{\Psi}_N\gamma^5\gamma^\mu\vec{\tau}\Psi_N] \cdot [\bar{\Psi}_N\gamma^5\gamma_\mu\vec{\tau}\Psi_N]. \quad (2)$$

The coupling strength parameter  $\alpha_{\text{IV-PV}} = 0.63 \text{ MeV fm}^3$  for DD-PCX [49] parametrization is obtained by minimizing the relative error  $\Delta \lesssim 1 \text{ MeV}$  between the experimentally determined  $M1$  peak position and theoretically calculated centroid energies for magic nuclei  $^{48}\text{Ca}$  and  $^{208}\text{Pb}$  [26,46]. Note that the pseudovector type of interaction has been modeled as a scalar product of two pseudovectors, which leads to the parity-violating mean field at the Hartree level. Thus, it does not make a contribution to the solution of natural-parity states, including the  $0^+$  nuclear ground state. However,  $\mathcal{L}_{\text{IV-PV}}$  has a finite contribution in the FT-RQRPA residual interactions for  $M1$  excitations.

At finite temperature, the occupation probabilities of single-particle states are given as

$$n_i = v_i^2(1 - f_i) + u_i^2 f_i, \quad (3)$$

where  $u_i$  and  $v_i$  are the BCS amplitudes. The temperature-dependent Fermi-Dirac distribution function is given by

$$f_i = [1 + \exp(E_i/k_B T)]^{-1}, \quad (4)$$

where  $k_B$  is the Boltzmann constant and  $T$  is the temperature. The quasiparticle energy of a state is given by

$$E_i = \sqrt{(\varepsilon_i - \lambda_q)^2 + \Delta_i^2}, \quad (5)$$

where  $\varepsilon_i$  denotes the single-particle energies and  $\lambda_q$  represents the chemical potentials for either proton or neutron states.  $\Delta_i$  refers to the pairing gap of the given state. A separable form of pairing interaction is introduced in both the FT-HBCS and FT-RQRPA approaches, also including the same relativistic

point-coupling interaction, DD-PCX [51]. The values of critical temperatures ( $T_c$ ), where the pairing correlations vanish, are calculated using the FT-HBCS with DD-PCX interaction. For instance, the  $T_c$  values of open-shell  $^{44}\text{Ca}$ ,  $^{52}\text{Ca}$ ,  $^{56}\text{Ca}$ ,  $^{64}\text{Ca}$ ,  $^{108}\text{Sn}$ ,  $^{116}\text{Sn}$ ,  $^{124}\text{Sn}$ , and  $^{140}\text{Sn}$  nuclei are obtained as 0.862, 0.528, 0.743, 0.700, 0.872, 0.834, 0.764, and 0.644 MeV, respectively.

The non-charge-exchange FT-RQRPA matrix is given by

$$\begin{pmatrix} \tilde{C} & \tilde{a} & \tilde{b} & \tilde{D} \\ \tilde{a}^+ & \tilde{A} & \tilde{B} & \tilde{b}^T \\ -\tilde{b}^+ & -\tilde{B}^* & -\tilde{A}^* & -\tilde{a}^T \\ -\tilde{D}^* & -\tilde{b}^* & -\tilde{a}^* & -\tilde{C}^* \end{pmatrix} \begin{pmatrix} \tilde{P} \\ \tilde{X} \\ \tilde{Y} \\ \tilde{Q} \end{pmatrix} = E_w \begin{pmatrix} \tilde{P} \\ \tilde{X} \\ \tilde{Y} \\ \tilde{Q} \end{pmatrix}, \quad (6)$$

where  $E_w$  denotes the excitation energies, and  $\tilde{P}$ ,  $\tilde{X}$ ,  $\tilde{Y}$ , and  $\tilde{Q}$  represent the corresponding eigenvectors, which are given by

$$\tilde{X}_{ab} = X_{ab} \sqrt{1 - f_a - f_b}, \quad (7)$$

$$\tilde{Y}_{ab} = Y_{ab} \sqrt{1 - f_a - f_b}, \quad (8)$$

$$\tilde{P}_{ab} = P_{ab} \sqrt{f_b - f_a}, \quad (9)$$

$$\tilde{Q}_{ab} = Q_{ab} \sqrt{f_b - f_a}. \quad (10)$$

The  $T$ -dependent matrix elements are given as

$$\begin{aligned} \tilde{A}_{abcd} &= \sqrt{1 - f_a - f_b} A'_{abcd} \sqrt{1 - f_c - f_d} \\ &+ (E_a + E_b) \delta_{ac} \delta_{bd}, \end{aligned} \quad (11)$$

$$\tilde{B}_{abcd} = \sqrt{1 - f_a - f_b} B_{abcd} \sqrt{1 - f_c - f_d}, \quad (12)$$

$$\begin{aligned} \tilde{C}_{abcd} &= \sqrt{f_b - f_a} C'_{abcd} \sqrt{f_d - f_c} \\ &+ (E_a - E_b) \delta_{ac} \delta_{bd}, \end{aligned} \quad (13)$$

$$\tilde{D}_{abcd} = \sqrt{f_b - f_a} D_{abcd} \sqrt{f_d - f_c}, \quad (14)$$

$$\tilde{a}_{abcd} = \sqrt{f_b - f_a} a_{abcd} \sqrt{1 - f_c - f_d}, \quad (15)$$

$$\tilde{b}_{abcd} = \sqrt{f_b - f_a} b_{abcd} \sqrt{1 - f_c - f_d}, \quad (16)$$

$$\tilde{a}_{abcd}^+ = \tilde{a}_{abcd}^T = \sqrt{f_d - f_c} a_{abcd}^+ \sqrt{1 - f_a - f_b}, \quad (17)$$

$$\tilde{b}_{abcd}^T = \tilde{b}_{abcd}^+ = \sqrt{f_d - f_c} b_{abcd}^T \sqrt{1 - f_a - f_b}, \quad (18)$$

where  $E_{a(b)}$  is the quasiparticle energy of the states obtained from the FT-HBCS results. The FT-QRPA equations were initially derived by Sommermann in Ref. [37], however, they were only applied to a schematic model. In the present work, we extend the FT-QRPA formalism from Ref. [37] by implementing the REDF with density-dependent point-coupling interactions for the study of the  $M1$  response at finite temperature. The detailed description of the FT-QRPA matrices is given in Refs. [37,39,40]. The FT-RQRPA matrix in Eq. (6) is diagonalized in a self-consistent way, allowing for a detailed analysis of each excitation on a state-by-state basis. We note that the  $A$  and  $B$  matrices contribute at  $T = 0$  and at  $T \neq 0$  as well; however, other matrix elements begin to contribute only at finite temperature due to the changes in occupation factors as well as the temperature factors. The reduced transition probability is given by

$$\begin{aligned} B(MJ) &= |\langle w || \hat{F}_J || \tilde{0} \rangle|^2 = \left| \sum_{c \geq d} \{ [\tilde{X}_{cd}^w + (-1)^{j_c - j_d + J} \tilde{Y}_{cd}^w] [u_c v_d + (-1)^J v_c u_d] \sqrt{1 - f_c - f_d} \right. \\ &\quad \left. + [\tilde{P}_{cd}^w + (-1)^{j_c - j_d + J} \tilde{Q}_{cd}^w] [u_c u_d - (-1)^J v_c v_d] \sqrt{f_d - f_c} \right\} \langle c || \hat{F}_J || d \rangle \Big|^2, \end{aligned} \quad (19)$$

where  $|w\rangle$  is the excited state and  $|\tilde{0}\rangle$  is the correlated FT-RQRPA vacuum state, and  $\hat{F}_J$  is the transition operator of the relevant excitation. To evaluate the magnetic dipole strength, we use the IV- $M1$  operator for the  $k$ th nucleon as

$$\hat{\mu}_w^{M1,IV} = \mu_N \sqrt{\frac{3}{4\pi}} \sum_{k \in A} [g_s^{IV} \hat{s}_w(k) + g_l^{IV} \hat{l}_w(k)] \hat{\tau}_0(k), \quad (20)$$

including the spin  $\hat{s}_w$  and the orbital angular momentum  $\hat{l}_w$ . The isospin convention is used as  $\hat{\tau}_0(k) = 1(-1)$  for protons (neutrons).  $\mu_N = e\hbar/(2m_N)$  denotes the nuclear magneton, and the nuclear spin and orbital  $g$  factors for the IV- $M1$  mode are  $g_s = 4.706$  and  $g_l = 0.5$  (see Refs. [26,52] for more details). The total  $M1$  transition strength can also be written in a compact form to identify the role of particular proton or neutron configurations,

$$B(M1, E_w) = \left| \sum_{c \geq d} [b_{cd}^\pi(E_w) + b_{cd}^\nu(E_w)] \right|^2. \quad (21)$$

Here,  $E_w$  is excitation energy obtained from the FT-RQRPA discrete  $M1$  spectra. The  $b_{cd}^\pi(E_w)$  and  $b_{cd}^\nu(E_w)$  represent the proton ( $\pi$ ) and neutron ( $\nu$ ) partial contributions for a specific configuration. The two-quasiparticle (2qp) cutoff energy for the configuration space  $E_{\text{cut}}$  is selected as 100 MeV, to provide a sufficient convergence in the  $M1$  excitation strength. For the presentation of the results, the discrete FT-RQRPA spectrum of  $M1$  response is smoothed with a Lorentzian function of  $\Gamma = 1.0$  MeV width [52].

### III. RESULTS

#### A. Calcium isotopes

The  $M1$  excitation at the leading one-body operator level would take place between the spin-orbit (SO) partner orbits, provided the independent single-particle picture is a good approximation [25]. Thus, the  $M1$  response provides important information on the underlying SO splittings. However, in the REDF framework, the  $M1$  properties depend not only on the SO splittings but also on the effects of the residual interaction

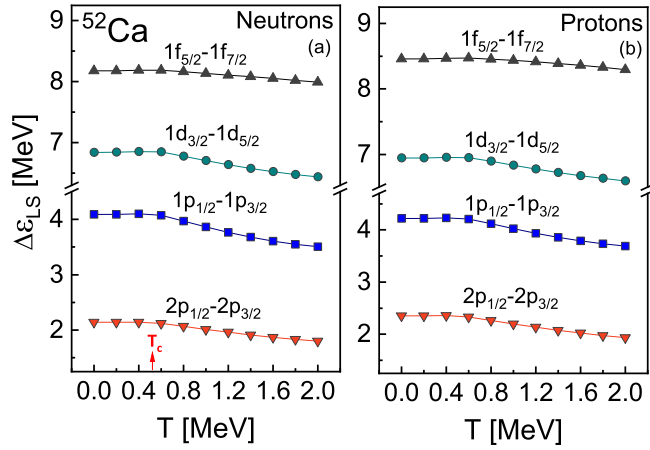


FIG. 1. The spin-orbit splitting energies  $\Delta\varepsilon_{LS}$  of neutron (a) and proton (b) configurations as a function of temperature for the  $^{52}\text{Ca}$  nucleus.

in the RQRPA [25]. The SO splitting energies are calculated as

$$\Delta\varepsilon_{LS} = \varepsilon_{nlj_{<}} - \varepsilon_{nlj_{>}}, \quad (22)$$

where  $(nlj)$  are the quantum numbers of major SO-partner single-particle states, and  $j_{<} = l - 1/2$  and  $j_{>} = l + 1/2$ . In Figs. 1(a) and 1(b), the SO splitting energies are displayed both for neutrons and protons as a function of temperature for  $^{52}\text{Ca}$ . We note that the single-particle energies can easily be affected by the inclusion of temperature in the calculations, which, in turn, modifies the SO splitting. It is clearly seen from Fig. 1 that the SO splitting energy is temperature dependent. While the SO splitting energy remains almost constant up to the critical temperature  $T_c = 0.528$  MeV, it gradually starts decreasing at higher temperatures. This reduction of the SO splitting energies above  $T_c$  will modify the  $M1$  response in both the low-energy and high-energy regions, as we will discuss below.

In Fig. 2, we display the  $M1$ -transition strength distributions of  $^{40-60}\text{Ca}$  nuclei with increasing temperature. First, we consider the results at  $T = 0$  MeV for  $^{40}\text{Ca}$  ( $Z, N = 20$ ), showing the absence of any  $M1$  response, as  $(1p_{3/2}, 1p_{1/2})$  and  $(1d_{5/2}, 1d_{3/2})$  states are fully occupied for protons and neutrons; therefore, no SO partners are available for the  $M1$  transition. Similarly, for  $^{60}\text{Ca}$  with  $N = 40$  neutrons, states up to  $1f_{5/2}$  and  $2p_{1/2}$  are fully occupied, and hence the  $M1$  transition is forbidden. Thus, no  $M1$  response is obtained for these two nuclei at zero temperature. For  $^{44-56}\text{Ca}$ , one can see a strong peak in each isotope that attributes to the  $M1$  excitation of valence neutron transitions  $\nu(1f_{7/2} \rightarrow 1f_{5/2})$ , whereas  $M1$  transitions are not present for protons due to the shell closure at  $Z = 20$ . A low-energy  $M1$  peak is also observed in  $^{52,56}\text{Ca}$  nuclei due to the  $\nu(2p_{3/2} \rightarrow 2p_{1/2})$  transition. More details about the evolution of  $M1$  strength along the  $^{40-60}\text{Ca}$  isotopic chain at zero temperature are given in Ref. [25].

Further, it is clearly evident from Fig. 2 that  $M1$ -transition strength distributions are sensitive to changes in temperature. At  $T = 0.5$  MeV, the results do not change much in Ca

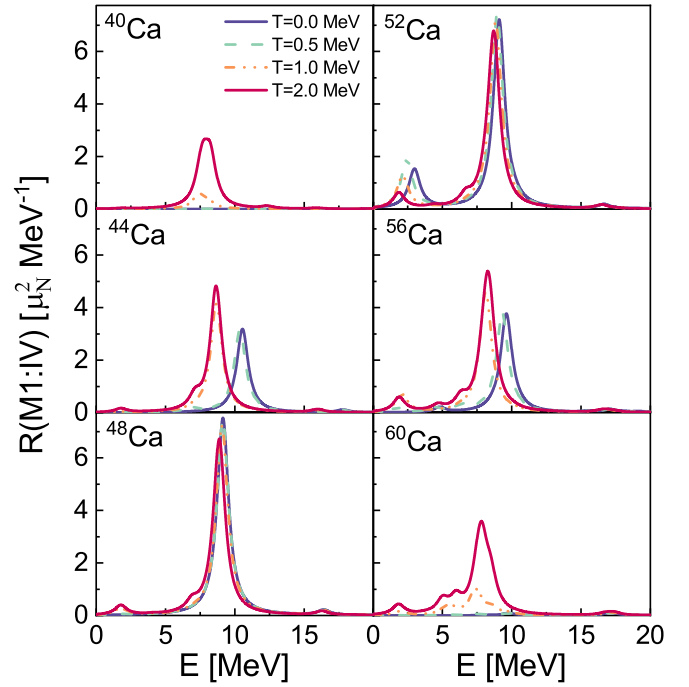


FIG. 2. The isovector  $M1$ -transition strength distributions of  $^{40-60}\text{Ca}$  isotopes, calculated using the FT-RQRPA at temperatures of  $T = 0, 0.5, 1,$  and  $2$  MeV.

isotopes. By increasing temperature further, at  $T = 1$  and  $2$  MeV, an interesting outcome is observed for the case of  $^{40}\text{Ca}$  and  $^{60}\text{Ca}$ . The  $M1$ -transition strength suddenly appears for these isotopes due to the emergence of new transitions in the  $\nu, \pi(1d_{5/2}, 1d_{3/2})$  and  $\nu, \pi(1f_{7/2}, 1f_{5/2})$  configurations. This occurs because particles are promoted to higher-energy orbits as a result of temperature effects, leading to the thermal unblocking of forbidden  $M1$  transitions. It is also noticed in Fig. 2 that the  $M1$  response shifts up to  $\approx 2$  MeV to the lower energies for  $^{44,48,52,56}\text{Ca}$  with increasing temperature. In addition to the decrease in the pairing correlations for open-shell nuclei and softening in the repulsive residual interaction, the changes in the  $M1$  response are also linked to the SO splitting energies, which reduce with increasing temperature, as shown in Fig. 1. Due to the thermal unblocking of states, new proton and neutron transitions also become possible in both high-energy ( $E > 5$  MeV) and low-energy ( $E < 5$  MeV) regions of open-shell nuclei  $^{44,48,52,56}\text{Ca}$ . In the high-energy region of these nuclei, proton and neutron  $(1f_{7/2} \rightarrow 1f_{5/2})$  transitions are the major contributors to the  $M1$  strength at  $T = 1$  and  $2$  MeV. A finite contribution from the  $\pi(1d_{5/2} \rightarrow 1d_{3/2})$  transition is also observed at  $T = 2$  MeV in  $^{40-60}\text{Ca}$  nuclei. Also, new smaller peaks arise in the low-energy region ( $E < 5$  MeV) of neutron-rich  $^{48-60}\text{Ca}$  isotopes as a result of neutron transitions, e.g.,  $\nu(2p_{3/2} \rightarrow 2p_{1/2})$  and  $\nu(1f_{7/2} \rightarrow 1f_{5/2})$ .

Tables I and II display the proton and neutron isovector partial contributions ( $b_{2qp}^{\pi(\nu)}$ ) to the  $M1$  transition strength, as defined in Eq. (21), for the  $^{52}\text{Ca}$  nucleus. Table I pertains to the high-energy region, whereas Table II is provided for the low-energy region. It is evident from the tables that the number of excitation energies and related contributing transitions in the

TABLE I. The isovector partial contributions  $b_{2qp}^{\pi(\nu)}$  ( $\mu_N$ ) of protons ( $\pi$ ) and neutrons ( $\nu$ ) to the dominant high-energy  $M1$  excitations in  $^{52}\text{Ca}$  nuclei at  $T = 0, 1$ , and 2 MeV are listed at corresponding excitation energies ( $E$ ). The total  $B(M1, E)$  values are obtained using Eq. (21), by summing over all proton and neutron configurations, also including those not listed in the table. The major contributions are highlighted in bold.

Configuration	$T = 0$ MeV	$T = 1$ MeV		$T = 2$ MeV		
	$E = 9.09$ MeV	$E = 8.84$ MeV	$E = 6.85$ MeV	$E = 8.71$ MeV	$E = 8.24$ MeV	$E = 6.68$ MeV
$\nu(1f_{7/2} \rightarrow 1f_{5/2})$	<b>-3.363</b>	<b>-3.207</b>	<b>0.216</b>	<b>-2.397</b>	<b>-1.694</b>	<b>0.382</b>
$\nu(2p_{3/2} \rightarrow 2p_{1/2})$	-0.029	-0.012	-0.003	-0.005		-0.003
$\nu(1f_{5/2} \rightarrow 2f_{7/2})$		-0.006		0.012	0.021	-0.003
$\nu(1g_{9/2} \rightarrow 2g_{7/2})$		-0.002		-0.082	0.039	0.004
$\pi(1f_{7/2} \rightarrow 1f_{5/2})$		<b>-0.117</b>	0.005	<b>-0.615</b>	<b>1.009</b>	0.060
$\pi(1d_{5/2} \rightarrow 1d_{3/2})$		-0.027	<b>-0.557</b>	<b>-0.115</b>	-0.028	<b>-1.189</b>
Total $B(M1, E)$ ( $\mu_N^2$ )	11.262	11.032	0.115	10.045	0.416	0.565

$M1$  response increases as one moves from  $T = 0$  to 2 MeV, signifying the thermal unblocking of transitions. The reduced transition probability for a specific excited state, denoted as  $B(M1, E)$ , is determined by summing up the contributions of each configuration while considering their relative signs. First, we observe that temperature leads to the fragmentation of the excited states, impacts the contribution of the main configurations, and causes a decrease in the total  $B(M1, E)$  value for a particular state with increasing temperature. Second, we find that new states appear; however, the contributions of these new configurations either are too small or they interfere destructively, which, in turn, results in low strength. While temperature leads to the scattering of nucleons into the continuum, this effect is less pronounced for protons due to the Coulomb barrier. Hence, neutron transitions dominate in the low-energy region of  $M1$  strength for neutron-rich Ca nuclei.

For further illustration, Figure 3 displays the temperature dependence of the major high-energy  $E_{\text{peak}}^{\text{High}}$  and low-energy  $E_{\text{peak}}^{\text{Low}}$  peaks in the  $M1$  strength distribution for  $^{52}\text{Ca}$ . In this case,  $\nu(1f_{7/2}, 1f_{5/2})$  and  $\nu(2p_{3/2}, 2p_{1/2})$  transitions are the primary contributors to the high-energy and low-energy peaks, respectively. Therefore, in Fig. 3, the SO splitting energies  $\Delta\epsilon_{\text{LS}}$  of these two respective configurations are shown for comparison relative to the  $M1$  excitation energies. For the  $E_{\text{peak}}^{\text{High}}$ , we observe a decrease around the critical temperature  $T_c = 0.528$  MeV, which then continues to decrease gradually with increasing temperature. The SO splitting energy also decreases slightly. Although the impact of pairing is subtle

in this region, its effect can be seen in the comparably rapid decrease in energy around the critical temperature. At higher temperatures, the slight decrease in  $E_{\text{peak}}^{\text{High}}$  is mainly related to the decrease in the SO splitting energy and weakening of the repulsive residual interaction. On the other hand, we observe a rapid decrease in  $E_{\text{peak}}^{\text{Low}}$  near the critical temperature, which is similar to the pairing phase transition, demonstrating the subtle interplay between the temperature effects and pairing correlations. Although the SO splitting energies are obtained as almost constant up to  $T_c$ , the decrease in the pairing correlations with increasing temperature leads to a sharp reduction of the energy. In other words, the pairing plays a significant role in the low-energy region of the  $M1$  response of open-shell nuclei below  $T_c$ . At higher temperatures,  $E_{\text{peak}}^{\text{Low}}$  continues to gradually decrease, but at a faster rate compared to  $E_{\text{peak}}^{\text{High}}$  since the SO splitting energy of the relevant transition decreases more rapidly.

Next, we study the non-energy-weighted  $m_0$  and energy-weighted  $m_1$  moments of the  $M1$  transition strength, calculated using the FT-RQRPA method. In Fig. 4, we can see the behavior of  $m_0$  [panel (a)] and  $m_1$  [panel (b)] as a function of the mass number  $A$  for Ca isotopes at temperatures ranging from  $T = 0$  to 2 MeV. The  $M1$  response does not appear when the SO partner states are either fully occupied or completely empty, a characteristic stemming from the use of the one-body operator in Eq. (20). Consequently, the  $M1$  response is absent at  $T = 0$  MeV in  $^{40,60}\text{Ca}$  and appears predominantly in other Ca isotopes through neutron transitions,

TABLE II. Same as Table I, but for the low-energy  $M1$  excitations in the  $^{52}\text{Ca}$  nucleus for  $E < 5$  MeV.

Configuration	$T = 0$ MeV	$T = 1$ MeV	$T = 2$ MeV	
	$E = 2.98$ MeV	$E = 2.14$ MeV	$E = 4.36$ MeV	$E = 1.86$ MeV
$\nu(2p_{3/2} \rightarrow 2p_{1/2})$	<b>-1.726</b>	<b>1.520</b>	-0.002	<b>1.057</b>
$\nu(1f_{7/2} \rightarrow 1f_{5/2})$	<b>0.192</b>	<b>-0.123</b>	0.028	-0.067
$\nu(1g_{9/2} \rightarrow 1g_{7/2})$			<b>-0.364</b>	-0.002
$\pi(1d_{5/2} \rightarrow 1d_{3/2})$		-0.006	0.005	-0.018
$\pi(1f_{7/2} \rightarrow 1f_{5/2})$		-0.004	0.004	-0.013
$\pi(2p_{3/2} \rightarrow 2p_{1/2})$				-0.012
Total $B(M1, E)$ ( $\mu_N^2$ )	2.336	1.923	0.108	0.892

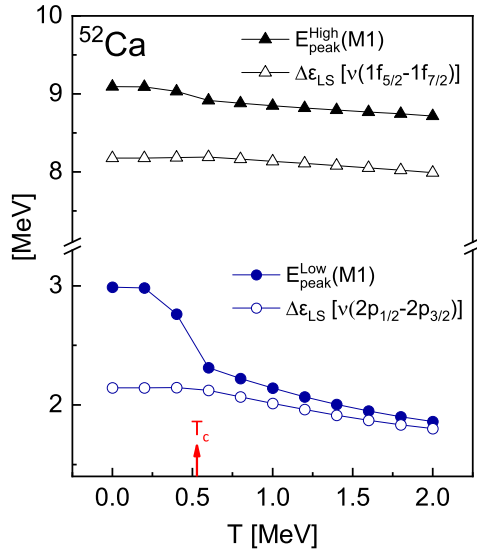


FIG. 3. Major high-energy ( $E_{\text{peak}}^{\text{High}}$ ) and low-energy ( $E_{\text{peak}}^{\text{Low}}$ )  $M1$  peak excitation energies, along with the SO splitting energies ( $\Delta\epsilon_{\text{LS}}$ ) of the respective primary contributing neutron configurations in  $^{52}\text{Ca}$ . The results are shown as a function of temperature in the range from  $T = 0$  to 2 MeV.

e.g.,  $\nu(1f_{7/2} \rightarrow 1f_{5/2})$ . It can be seen from Figs. 4(a) and 4(b) that the moments  $m_0$  and  $m_1$  have the highest magnitudes for  $^{48}\text{Ca}$  and  $^{52}\text{Ca}$ , since the  $\nu(1f_{7/2})$  [and  $\nu(2p_{3/2})$  for  $^{52}\text{Ca}$ ] state is nearly filled, and the corresponding  $M1$  excitation strength is higher. For heavier isotopes of  $^{56,60}\text{Ca}$ , as the  $\nu(1f_{5/2})$  state begins to fill, the transition strength decreases due to the blocking of the  $\nu(1f_{7/2} \rightarrow 1f_{5/2})$  transition, as can be seen in Figs. 2 and 4 at zero temperature. Similar results are also obtained in Ref. [25].

With the increase in temperature, the  $m_0$  and  $m_1$  moments of  $^{40,60}\text{Ca}$  nuclei show a rapid increase above  $T = 0.8$  MeV due to the opening of new proton and neutron excitation channels. Although it is less pronounced compared to  $^{40}\text{Ca}$  and  $^{60}\text{Ca}$ , we also obtain an increase in the moments of  $^{44}\text{Ca}$  and  $^{56}\text{Ca}$  at higher temperatures. These results are also consistent with the results obtained in observation of Fig. 2 and illustrate substantial contributions of new transitions which become allowed at higher temperatures. On the other hand, we obtain a moderate decrease in the moments for  $^{48}\text{Ca}$  and  $^{52}\text{Ca}$  at high temperatures. The main reason for the decrease in the  $m_0$  and  $m_1$  moments in  $^{48}\text{Ca}$  and  $^{52}\text{Ca}$  is the impact of the temperature on the  $\nu(1f_{7/2})$  and  $\nu(2p_{3/2})$  states. As can be seen from Tables I and II, the contribution of the  $\nu(1f_{7/2}, 1f_{5/2})$  and  $\nu(2p_{3/2}, 2p_{1/2})$  transitions to the  $M1$  strength decreases substantially with increasing temperature, and the contribution of the new states is found to be subtle since their partial magnitudes are small and interfere destructively, resulting in a decrease in the  $M1$  strength.

### B. Tin isotopes

The temperature dependence of isovector  $M1$  strength distributions is also systematically studied in even-even  $^{100-140}\text{Sn}$  isotopes, as shown in Fig. 5. First, we consider the

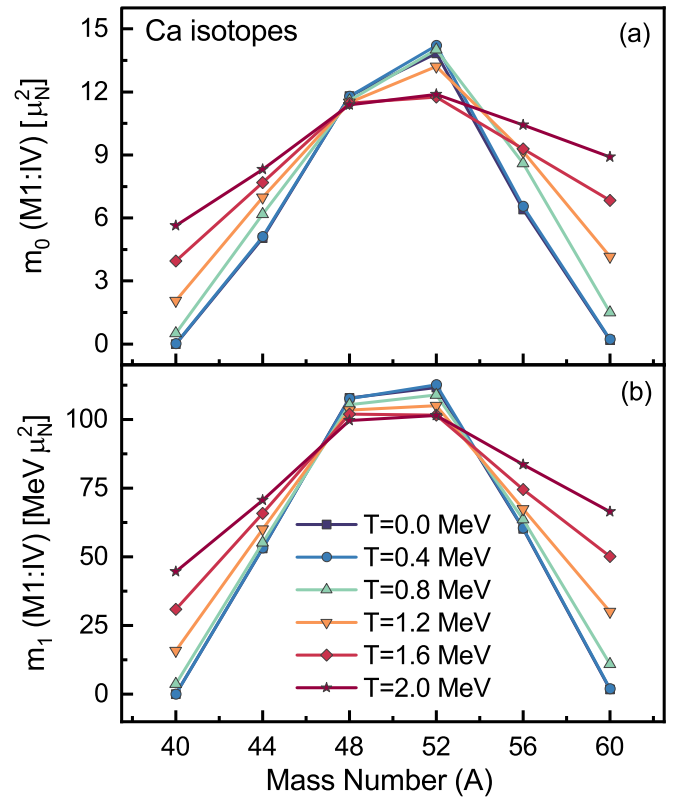


FIG. 4. (a) Non-energy-weighted  $m_0$  and (b) energy-weighted  $m_1$  moments of  $M1$  response in  $^{40-60}\text{Ca}$  between  $T = 0-2$  MeV.

$T = 0$  MeV case. The  $M1$  excitations are expected due to the proton  $\pi(1g_{9/2} \rightarrow 1g_{7/2})$  and the neutron  $\nu(1g_{9/2} \rightarrow 1g_{7/2})$ ,  $\nu(2d_{5/2} \rightarrow 2d_{3/2})$ , and/or  $\nu(1h_{11/2} \rightarrow 1h_{9/2})$  transitions until the higher state in the SO configuration becomes fully occupied to block the  $M1$  transitions. In closed-shell nuclei  $^{100}\text{Sn}$  and  $^{132}\text{Sn}$ , the pairing correlations do not contribute; hence, the  $M1$  excitation energy is determined mainly by the SO splitting energy as well as the residual interaction. For  $^{100}\text{Sn}$  at zero temperature, the  $M1$  strength is obtained as a single peak at 9.47 MeV, which is mainly formed with the proton and neutron ( $1g_{9/2}$  and  $1g_{7/2}$ ) transitions. As the number of neutrons increases along the Sn isotope chain, the  $M1$  response exhibits two peaks in the high-energy region. The first peak at lower energy is primarily due to proton transitions, while the second, at higher energy, is dominated by neutron transitions. Similar results are obtained for the  $T = 0.5$  MeV case, where the  $M1$  strength distribution shifts slightly to the lower energies, as shown in Fig. 5. A thorough study of  $M1$  transitions in  $^{100-136}\text{Sn}$  isotopes has been carried out at  $T = 0$  MeV using the RQRPA framework, and a detailed description is given in Ref. [27].

Similar to the findings in Ca isotopes, the  $M1$  strength starts to shift downward, and new excited states appear in both the low-energy and high-energy regions with increasing temperature. Besides the downward shift in the  $M1$  strength, we also observe a change in the  $^{108,124,140}\text{Sn}$  nuclei from a two-peak to a single-peak structure of  $M1$  strength as the temperature increases. Due to the vanishing of pairing

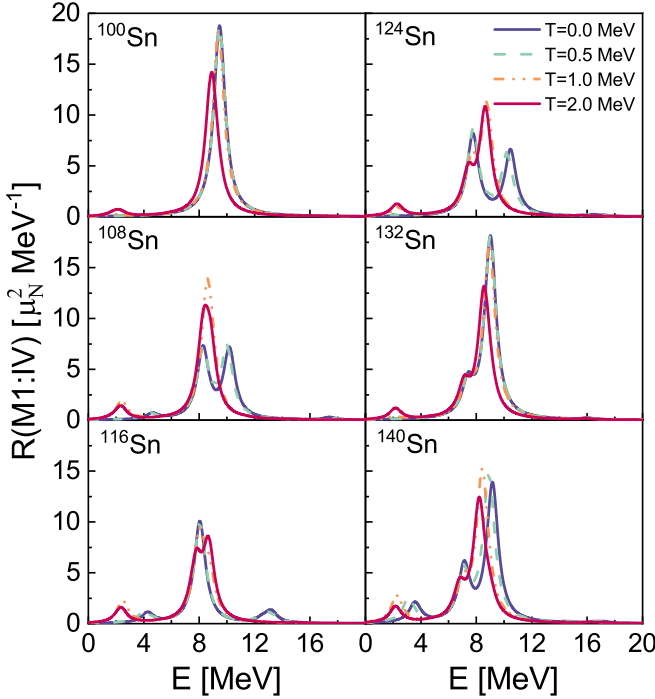


FIG. 5. The same as in Fig. 2, but for  $^{100-140}\text{Sn}$  isotopes.

correlations at critical temperatures, the configuration energies between the proton and neutron components start to approach one another, which results in the merging of two peaks into a single peak at higher temperatures. To elucidate further, the structure of  $M1$  strength distributions at finite temperatures is explored by analyzing all transitions that contribute to these states for each considered Sn nucleus at  $T = 1$  and 2 MeV. This study has revealed that along with the major  $\nu, \pi(1g_{9/2} \rightarrow 1g_{7/2})$  transitions,  $\nu, \pi(1h_{11/2} \rightarrow 1h_{9/2})$  transitions also start contributing in the high-energy region of  $^{100-140}\text{Sn}$  nuclei at higher temperatures. Finite contributions from  $\nu(1i_{13/2} \rightarrow 2i_{11/2})$  and  $\nu(1h_{9/2} \rightarrow 2h_{11/2})$  transitions are also obtained in the neutron-rich Sn isotopes due to the thermal unblocking. Moreover, a new low-energy  $M1$  peak below  $E = 5$  MeV appears in all Sn isotopes at finite temperatures. In the lower-mass Sn isotopes, the  $\nu(2d_{5/2} \rightarrow 2d_{3/2})$

TABLE IV. Same as Table I but for the low-energy  $M1$  excitations in  $^{140}\text{Sn}$  nucleus.

Configuration	$T = 0$ MeV	$T = 1$ MeV	$T = 2$ MeV
	$E = 3.57$ MeV	$E = 2.26$ MeV	$E = 2.17$ MeV
$\nu(2f_{7/2} \rightarrow 2f_{5/2})$	<b>2.078</b>	<b>-2.267</b>	<b>-1.434</b>
$\nu(1h_{11/2} \rightarrow 1h_{9/2})$	-0.138	0.102	0.079
$\nu(2d_{5/2} \rightarrow 2d_{3/2})$			<b>-0.166</b>
$\pi(2d_{5/2} \rightarrow 2d_{3/2})$		-0.016	-0.131
$\pi(1g_{9/2} \rightarrow 1g_{7/2})$	<b>-0.267</b>	<b>0.155</b>	0.092
Total $B(M1, E)$ ( $\mu_N^2$ )	2.815	4.088	2.403

transition is the major contributor to the low-energy peak, and the  $\nu(2f_{7/2} \rightarrow 2f_{5/2})$  transition also begins contributing in the neutron-rich nuclei. A thorough analysis of the partial contributions of protons and neutrons in the high-energy ( $E > 5$  MeV) and low-energy ( $E < 5$  MeV) regions is given in Tables III and IV, respectively, for the neutron-rich  $^{140}\text{Sn}$  nucleus at  $T = 0, 1, \text{ and } 2$  MeV.

This investigation extends further to the  $M1$  non-energy-weighted  $m_0$  and energy-weighted  $m_1$  summations, along with the centroid energies ( $E_c = m_1/m_0$ ), as functions of temperature for  $^{100-140}\text{Sn}$  isotopes, as shown in Fig. 6. Figures 6(a)–6(c) display moments for the low-energy region ( $E < 5$  MeV), while Figs. 6(d)–6(f) represent these summations for the high-energy region ( $E > 5$  MeV). This energy cutoff is selected because it clearly separates the low- and high-energy regions in the  $M1$  strength distributions for all Sn isotopes, as shown in Fig. 5. We then elaborate on the variation of moments in the low-energy region with increasing temperature, as presented in Figs. 6(a)–6(c). For closed-shell  $^{100,132}\text{Sn}$  nuclei, the moments and centroid energy remain nearly zero up to  $T = 0.8$  MeV because the spin-orbit partner states are unavailable for  $M1$  transitions in the low-energy region. Then,  $E_c$  values increase linearly with temperature due to the thermal unblocking of these states. The rate of increase in the moments is higher for  $^{132}\text{Sn}$  compared to  $^{100}\text{Sn}$  because it is neutron-rich, and with increasing temperature particles are more easily scattered to the continuum region. Additionally, we observed a slight increase in the centroid energies with increasing temperature. However, the behavior of the  $m_0$

TABLE III. Same as Table I but for the high-energy  $M1$  excitations in  $^{140}\text{Sn}$  nucleus. The excitation energies ( $E$ ) are given in units of MeV.

Configuration	$T = 0$ MeV		$T = 1$ MeV			$T = 2$ MeV				
	$E = 7.12$	$E = 9.16$	$E = 6.97$	$E = 8.41$	$E = 8.46$	$E = 6.79$	$E = 8.04$	$E = 8.20$	$E = 8.27$	$E = 8.98$
$\nu(1h_{11/2} \rightarrow 1h_{9/2})$	<b>-1.049</b>	<b>3.664</b>	<b>1.136</b>	<b>2.382</b>	<b>-2.743</b>	<b>1.041</b>	<b>-1.857</b>	<b>2.301</b>	<b>-1.963</b>	<b>0.437</b>
$\nu(2f_{7/2} \rightarrow 2f_{5/2})$	0.062	0.046	-0.019	0.013	-0.013	-0.008	-0.003	0.006	-0.005	0.003
$\nu(2f_{7/2} \rightarrow 3f_{5/2})$	-0.020	0.037	0.031	0.016	-0.016	0.014	-0.007	0.012	-0.009	0.003
$\nu(1h_{9/2} \rightarrow 2h_{11/2})$	0.001		-0.003	-0.028			-0.013	<b>0.111</b>	<b>0.145</b>	-0.003
$\nu(1i_{13/2} \rightarrow i_{11/2})$			-0.008	0.004	-0.003	-0.049	-0.008	0.015	-0.013	0.005
$\nu(1i_{13/2} \rightarrow 2i_{11/2})$	-0.001		0.005	-0.029	0.031	0.022	0.038	-0.087	0.089	<b>0.890</b>
$\pi(1g_{9/2} \rightarrow 1g_{7/2})$	<b>3.913</b>	<b>0.828</b>	<b>-3.227</b>	<b>0.748</b>	<b>-0.806</b>	<b>-3.183</b>	<b>-0.281</b>	<b>0.505</b>	<b>-0.477</b>	<b>0.158</b>
$\pi(1h_{11/2} \rightarrow 1h_{9/2})$				0.006		0.029	<b>0.609</b>	<b>0.298</b>	<b>-0.179</b>	0.019
Total $B(M1, E)$ ( $\mu_N^2$ )	8.448	20.585	4.420	9.627	12.403	4.647	2.313	9.979	5.811	2.281



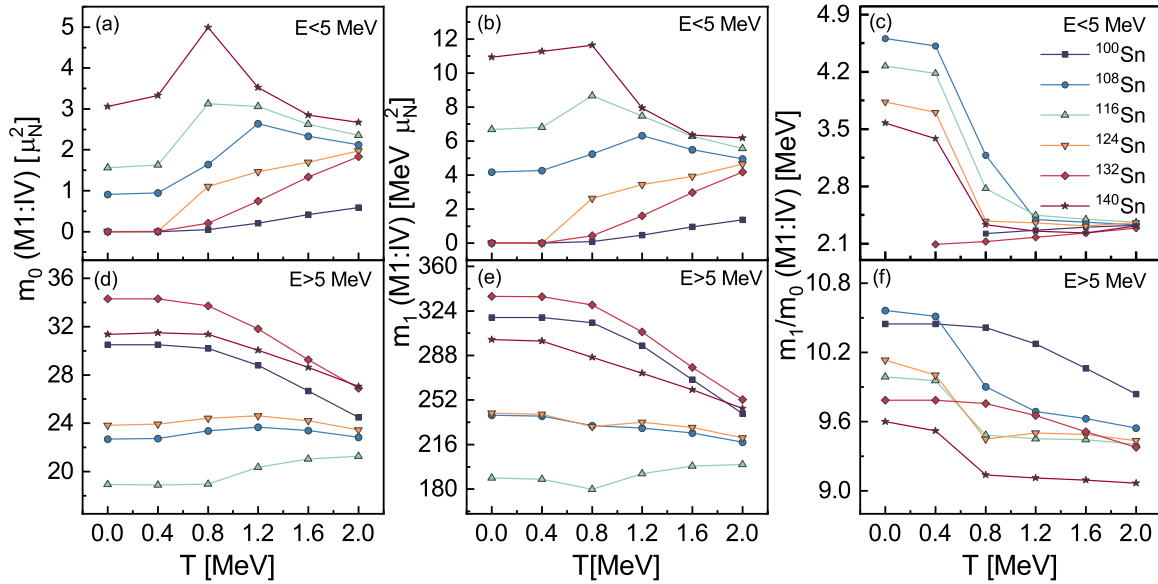


FIG. 6. The isovector  $M1$  non-energy-weighted sum  $m_0$ , the energy-weighted sum  $m_1$ , and the centroid energy ( $m_1/m_0$ ) in  $^{100-140}\text{Sn}$  for the low-energy region ( $E < 5$  MeV) [panels (a)–(c)] and the high-energy region ( $E > 5$  MeV) [panels (d)–(f)] as a function of temperature.

and  $m_1$  moments in open-shell nuclei with increasing temperature is not straightforward and displays dependence on the particular shell structure. In all open-shell nuclei, a sharp increase is observed in the moments above  $T = 0.4$  MeV and up to the critical temperatures. This change is mainly related to the decrease in the pairing correlations. At higher temperatures, pairing correlations disappear and a decrease is observed in the  $m_0$  and  $m_1$  moments for  $^{108,116,140}\text{Sn}$ . Only for  $^{124}\text{Sn}$ , the moments continue to increase with increasing temperature. For instance, in  $^{140}\text{Sn}$ , we found that the impact of the major configuration  $\nu(2f_{7/2} \rightarrow 2f_{5/2})$  decreases with increasing temperature due to the weakening of the residual interaction, and the partial contributions from the new configurations interfere destructively. As a result, we observe a decrease in the moments, as illustrated in Table IV. Similar results are also obtained for  $^{108,116,140}\text{Sn}$ . For  $^{124}\text{Sn}$ , there is a negligible  $M1$  response below  $E < 5$  MeV at very low temperatures due to the inaccessibility of single-particle partners for  $M1$  transitions in the low-energy region. However, due to thermal unblocking, new excitation channels primarily emerge between the  $\nu(2d_{5/2}, 2d_{3/2})$  configurations, and the sum of moments  $m_0$  and  $m_1$  also increases with temperature. It is also observed that the difference between the  $m_0$  and  $m_1$  moments of different nuclei decrease as the shell effects diminish at higher temperatures. Finally, the centroid energy first decreases sharply up to the critical temperatures and then exhibits only slight changes as the temperature increases further.

In the high-energy region ( $E > 5$  MeV), the isovector variables  $m_0$ ,  $m_1$ , and  $E_c$  smoothly reduce for closed-shell nuclei  $^{100,132}\text{Sn}$ . This means that at higher temperatures, a portion of the  $M1$  strength shifts to the low-energy region. However, a transition in the variation of moments and centroid energies is observed around  $T \approx 0.8$  MeV (or critical temperatures) for open-shell Sn isotopes in the high-energy region. At higher temperatures, we observed either a slight increase or a slight decrease in the  $m_0$  and  $m_1$  moments, depending on the par-

ticular nuclei. For all open-shell nuclei, the centroid energy decreases with increasing temperature up to the critical point, after which it changes only slightly with further temperature increases. As discussed earlier in the explanation of Fig. 5, this transition occurs due to the interplay of pairing and thermal effects. The behavior of the  $M1$  strength is governed by subtle effects related to single-particle structure, pairing correlations, respective occupation probabilities, and the FT-RQRPA residual interaction.

#### IV. SUMMARY

A novel approach, the self-consistent FT-RQRPA framework based on the relativistic energy density functional, has been applied to study the temperature dependence of isovector  $M1$  excitations. The properties of  $^{40-60}\text{Ca}$  and  $^{100-140}\text{Sn}$  isotopes were calculated at finite temperatures within the relativistic framework using the FT-HBCS method with the DD-PCX functional and separable pairing interaction. The FT-RQRPA is extended for the study of unnatural parity excitations of  $M1$  type.

By employing the FT-HBCS method, we studied the evolution of spin-orbit (SO) splitting energies in the open-shell nucleus  $^{52}\text{Ca}$  at temperatures both below and above the critical temperature  $T_c$ . We observed a reduction in the spin-orbit splitting energies as the temperature increased. The FT-RQRPA calculation of the  $M1$  response in both Ca and Sn isotopes showed a systematic shift of the strength distributions to lower energies in both Ca and Sn isotope chains as the temperature increased. The changes in the  $M1$  response are influenced not only by the weakening and disappearance of the pairing correlations and the softening of the repulsive residual interaction but also by the decreasing SO splitting energies. Remarkably, we found that  $M1$  strength suddenly emerges as the temperature increases in nuclei with initially blocked  $M1$  transitions. This phenomenon is attributed to the

thermal unblocking of new proton and neutron excitations between the spin-orbit partner states. The thermal unblocking of states also results in the formation of new  $M1$  peaks in the low-energy region.

The results of our study are also quantitatively assessed by analyzing the temperature dependence of the non-energy-weighted sum ( $m_0$ ), the energy-weighted sum of the transition strength ( $m_1$ ), and the centroid energy in the considered isotope chains. The changes in the moments  $m_0$  and  $m_1$  of Ca and Sn nuclei with increasing temperature indicate that the isotopic evolution of the  $M1$  response lacks a uniform pattern, at least at low temperatures. This lack of uniformity can be attributed to the influence of multiple contributing factors, such as the particular shell structure, pairing correlations, and residual interaction. In general, we observe a sharp change in the variation of moments and centroid energies with temperature for open-shell Sn nuclei. This change results from a phase transition from a superfluid state to the normal state that occurs near the critical temperatures, where pairing effects decrease sharply. At high temperatures, the shell effects also diminish, and the differences between the  $m_0$  and  $m_1$  moments decrease for the considered isotope chains. In conclusion, we have found that temperature effects can considerably modify

the magnetic dipole response. Further studies on the possible contributions of magnetic transitions at finite temperature in the  $\gamma$ -strength functions for  $(n, \gamma)$  reactions are required. These studies are left for future work. The experimental data on  $M1$  excitations in hot nuclei is currently lacking due to the complexity of methods required to measure  $M1$  emissions in highly excited nuclei, which are weaker than  $E1$  transitions. However, certain experimental approaches, as discussed in the Introduction, with highly efficient  $\gamma$  detectors, can provide possibilities for investigation of  $M1$  emissions in hot nuclei. Thus, the experimental studies to assess the properties of  $M1$  emissions at finite temperature are called for.

#### ACKNOWLEDGMENTS

We would like to thank Dr. Oliver Wieland for discussions about the experimental studies in hot nuclei. This work is supported by the Croatian Science Foundation under the project Relativistic Nuclear Many-Body Theory in the Multimesenger Observation Era (Grant No. IP-2022-10-7773). E.Y. acknowledges support from the UK Science and Technology Facilities Council (STFC) through Grant No. ST/Y000013/1.

- 
- [1] K. Heyde, P. von Neumann-Cosel, and A. Richter, *Rev. Mod. Phys.* **82**, 2365 (2010).
  - [2] P. Vesely, J. Kvasil, V. O. Nesterenko, W. Kleinig, P. G. Reinhard, and V. Y. Ponomarev, *Phys. Rev. C* **80**, 031302(R) (2009).
  - [3] V. Tselyaev, N. Lyutorovich, J. Speth, P.-G. Reinhard, and D. Smirnov, *Phys. Rev. C* **99**, 064329 (2019).
  - [4] S. Goriely, S. Hilaire, S. Péru, M. Martini, I. Deloncle, and F. Lechaftois, *Phys. Rev. C* **94**, 044306 (2016).
  - [5] K. Langanke, G. Martínez-Pinedo, B. Müller, H.-T. Janka, A. Marek, W. R. Hix, A. Juodagalvis, and J. M. Sampaio, *Phys. Rev. Lett.* **100**, 011101 (2008).
  - [6] H. Loens, K. Langanke, G. Martínez-Pinedo, and K. Sieja, *Eur. Phys. J. A* **48**, 34 (2012).
  - [7] S. Goriely, A. Bauswein, and H.-T. Janka, *Astrophys. J. Lett.* **738**, L32 (2011).
  - [8] N. Ryezayeva, T. Hartmann, Y. Kalmykov, H. Lenske, P. von Neumann-Cosel, V. Y. Ponomarev, A. Richter, A. Shevchenko, S. Volz, and J. Wambach, *Phys. Rev. Lett.* **89**, 272502 (2002).
  - [9] S. Joly, D. M. Drake, and L. Nilsson, *Phys. Rev. C* **20**, 2072 (1979).
  - [10] M. Igashira, H. Kitazawa, M. Shimizu, H. Komano, and N. Yamamuro, *Nucl. Phys. A* **457**, 301 (1986).
  - [11] M. Guttormsen, J. Rekstad, A. Henriquez, F. Ingebretsen, and T. F. Thorsteinsen, *Phys. Rev. Lett.* **52**, 102 (1984).
  - [12] P. Axel, *Phys. Rev.* **126**, 671 (1962).
  - [13] S. Goriely, *Phys. Lett. B* **436**, 10 (1998).
  - [14] P. Fanto and Y. Alhassid, [arXiv:2112.13772](https://arxiv.org/abs/2112.13772).
  - [15] Y. Beaujeault-Taudière, M. Frosini, J.-P. Ebran, T. Duguet, R. Roth, and V. Somà, *Phys. Rev. C* **107**, L021302 (2023).
  - [16] M. Guttormsen, R. Chankova, U. Agvaanluvsan, E. Algin, L. A. Bernstein, F. Ingebretsen, T. Lönnroth, S. Messelt, G. E. Mitchell, J. Rekstad, A. Schiller, S. Siem, A. C. Sunde, A. Voinov, and S. Ødegård, *Phys. Rev. C* **71**, 044307 (2005).
  - [17] M. Krtička, F. Bečvář, J. Honzátko, I. Tomandl, M. Heil, F. Käppeler, R. Reifarth, F. Voss, and K. Wisshak, *Phys. Rev. Lett.* **92**, 172501 (2004).
  - [18] A. Voinov, E. Algin, U. Agvaanluvsan, T. Belgya, R. Chankova, M. Guttormsen, G. E. Mitchell, J. Rekstad, A. Schiller, and S. Siem, *Phys. Rev. Lett.* **93**, 142504 (2004).
  - [19] R. Schwengner, S. Frauendorf, and A. C. Larsen, *Phys. Rev. Lett.* **111**, 232504 (2013).
  - [20] N. Lo Iudice and F. Palumbo, *Phys. Rev. Lett.* **41**, 1532 (1978).
  - [21] D. Bohle, A. Richter, W. Steffen, A. Dieperink, N. Lo Iudice, F. Palumbo, and O. Scholten, *Phys. Lett. B* **137**, 27 (1984).
  - [22] D. Bohle, G. Kuchler, A. Richter, and W. Steffen, *Phys. Lett. B* **148**, 260 (1984).
  - [23] N. Pietralla, P. von Brentano, R.-D. Herzberg, U. Kneissl, N. Lo Iudice, H. Maser, H. H. Pitz, and A. Zilges, *Phys. Rev. C* **58**, 184 (1998).
  - [24] T. Oishi, A. Ravlić, and N. Paar, *Phys. Rev. C* **105**, 064309 (2022).
  - [25] T. Oishi, G. Krui, and N. Paar, *J. Phys. G: Nucl. Part. Phys.* **47**, 115106 (2020).
  - [26] G. Kružić, T. Oishi, D. Vale, and N. Paar, *Phys. Rev. C* **102**, 044315 (2020).
  - [27] G. Kružić, T. Oishi, and N. Paar, *Phys. Rev. C* **103**, 054306 (2021).
  - [28] T. Oishi, G. Kružić, and N. Paar, *Eur. Phys. J. A* **57**, 180 (2021).
  - [29] P. Bortignon, A. Bracco, and R. Broglia, *Giant Resonances: Nuclear Structure at Finite Temperature*, Contemporary Concepts in Physics (CRC Press, Boca Raton, Florida, 1998).
  - [30] D. Santonocito and Y. Blumenfeld, *Eur. Phys. J. A* **56**, 279 (2020).
  - [31] O. Wieland, A. Bracco, F. Camera, G. Benzoni, N. Blasi, S. Brambilla, F. Crespi, A. Giussani, S. Leoni, P. Mason, B. Million, A. Moroni, S. Barlini, V. L. Kravchuk, F. Gramegna,

- A. Lanchais, P. Mastinu, A. Maj, M. Brekiesz, M. Kmiecik *et al.*, *Phys. Rev. Lett.* **97**, 012501 (2006).
- [32] T. Baumann, E. Ramakrishnan, A. Azhari, J. Beene, R. Charity, J. Dempsey, M. Halbert, P.-F. Hua, R. Kryger, P. Mueller, R. Pfaff, D. Sarantites, L. Sobotka, D. Stracener, M. Thoennessen, G. Van Buren, R. Varner, and S. Yokoyama, *Nucl. Phys. A* **635**, 428 (1998).
- [33] E. Ramakrishnan, T. Baumann, A. Azhari, R. A. Kryger, R. Pfaff, M. Thoennessen, S. Yokoyama, J. R. Beene, M. L. Halbert, P. E. Mueller, D. W. Stracener, R. L. Varner, R. J. Charity, J. F. Dempsey, D. G. Sarantites, and L. G. Sobotka, *Phys. Rev. Lett.* **76**, 2025 (1996).
- [34] S. Mukhopadhyay, D. Pandit, S. Pal, S. Bhattacharya, A. De, S. Bhattacharya, C. Bhattacharya, K. Banerjee, S. Kundu, T. Rana, G. Mukherjee, R. Pandey, M. Gohil, H. Pai, J. Meena, and S. Banerjee, *Phys. Lett. B* **709**, 9 (2012).
- [35] M. Guttormsen, T. Ramsøy, and J. Rekstad, *Nucl. Instrum. Methods Phys. Res., Sect. A* **255**, 518 (1987).
- [36] A. C. Larsen, M. Guttormsen, M. Krtička, E. Běták, A. Bürger, A. Görge, H. T. Nyhus, J. Rekstad, A. Schiller, S. Siem, H. K. Toft, G. M. Tveten, A. V. Voinov, and K. Wikan, *Phys. Rev. C* **83**, 034315 (2011).
- [37] H. M. Sommermann, *Ann. Phys.* **151**, 163 (1983).
- [38] E. Khan, N. Van Giai, and M. Grasso, *Nucl. Phys. A* **731**, 311 (2004).
- [39] E. Yüksel, G. Colò, E. Khan, Y. F. Niu, and K. Bozkurt, *Phys. Rev. C* **96**, 024303 (2017).
- [40] E. Yüksel, G. Colo, E. Khan, and Y. Niu, *Eur. Phys. J. A* **55**, 230 (2019).
- [41] Y. Niu, N. Paar, D. Vretenar, and J. Meng, *Phys. Lett. B* **681**, 315 (2009).
- [42] E. Litvinova and N. Belov, *Phys. Rev. C* **88**, 031302(R) (2013).
- [43] E. Litvinova and H. Wibowo, *Phys. Rev. Lett.* **121**, 082501 (2018).
- [44] E. Litvinova and H. Wibowo, *Eur. Phys. J. A* **55**, 223 (2019).
- [45] A. Kaur, E. Yüksel, and N. Paar, *Phys. Rev. C* **109**, 014314 (2024).
- [46] G. Kružić, T. Oishi, and N. Paar, *Eur. Phys. J. A* **59**, 50 (2023).
- [47] A. L. Goodman, *Nucl. Phys. A* **352**, 30 (1981).
- [48] E. Yüksel, E. Khan, K. Bozkurt, and G. Colò, *Eur. Phys. J. A* **50**, 160 (2014).
- [49] E. Yüksel, T. Marketin, and N. Paar, *Phys. Rev. C* **99**, 034318 (2019).
- [50] T. Nikšić, N. Paar, D. Vretenar, and P. Ring, *Comput. Phys. Commun.* **185**, 1808 (2014).
- [51] Y. Tian, Z.-Y. Ma, and P. Ring, *Phys. Rev. C* **80**, 024313 (2009).
- [52] N. Paar, P. Ring, T. Nikšić, and D. Vretenar, *Phys. Rev. C* **67**, 034312 (2003).